

1 **Reduced-complexity air quality intervention modelling** 2 **over China: development of the InMAPv1.6.1-China and** 3 **comparison with the CMAQv5.2 model**

4 Ruili Wu^{1,2}, Christopher W. Tessum³, Yang Zhang⁴, Chaopeng Hong⁵, Yixuan Zheng⁶,
5 Xinyin Qin¹, Shigan Liu¹, and Qiang Zhang¹

6 ¹Ministry of Education Key Laboratory for Earth System Modelling, Department of Earth System
7 Science, Tsinghua University, Beijing 100084, China

8 ²State Environmental Protection Key Laboratory of Quality Control in Environmental Monitoring, China
9 National Environmental Monitoring Centre, Beijing 100012, China

10 ³Department of Civil and Environmental Engineering, the University of Illinois at Urbana-Champaign,
11 Urbana, Illinois 61801, United States

12 ⁴Department of Civil and Environmental Engineering, Northeastern University, Boston, Massachusetts
13 02115, United States

14 ⁵Institute of Environment and Ecology, Tsinghua Shenzhen International Graduate School, Tsinghua
15 University, Shenzhen 518055, China

16 ⁶Center of Air Quality Simulation and System Analysis, Chinese Academy of Environmental Planning,
17 Beijing 100012, China

18 Correspondence to: Ruili Wu (wurl15@tsinghua.org.cn or wurl@cnemc.cn)

19 **Abstract.** This paper presents the first development and evaluation of the reduced-complexity air quality
20 model for China. In this study, a reduced-complexity air quality intervention model over China (InMAP-
21 China) is developed by linking a regional air quality model, a reduced-complexity air quality model, an
22 emission inventory database for China, and a health impact assessment model to rapidly estimate the air
23 quality and health impacts of emission sources in China. The modelling system is applied over mainland
24 China for 2017 under various emission scenarios. A comprehensive model evaluation is conducted by
25 comparison against conventional CMAQ simulations and ground-based observations. We found that
26 InMAP-China satisfactorily predicted total PM_{2.5} concentrations in terms of statistical performance.
27 Compared with the observed PM_{2.5} concentrations, the mean bias (MB), normalized mean bias (NMB),
28 and correlations of the total PM_{2.5} concentrations are -8.1 µg/m³, -18%, and 0.6, respectively. The
29 statistical performance is considered to be satisfactory for a reduced-complexity air quality model and
30 remains consistent with that evaluated in the United States. The underestimation of total PM_{2.5}
31 concentrations was mainly caused by its composition, primary PM_{2.5}. In terms of the ability to quantify
32 source contributions of PM_{2.5} concentrations, InMAP-China presents similar results in comparison with

33 those based on the CMAQ model, the difference is mainly caused by the different treatment of secondary
34 inorganic aerosols in the two models. Focusing on the health impacts, the annual PM_{2.5}-related premature
35 mortality estimated using InMAP-China in 2017 was 1.92 million, which was 25 ten thousand deaths
36 lower than estimated based on CMAQ simulations as a result of underestimation of PM_{2.5} concentrations.
37 This work presents a version of the reduced-complexity air quality model over China, provides a
38 powerful tool to rapidly assess the air quality and health impacts associated with control policy, and to
39 quantify the source contribution attributable to many emission sources.

40 **1 Introduction**

41 With rapid urbanization and industrialization, fine particulate matter pollution less than 2.5 μm in
42 diameter (PM_{2.5}) has become a major environmental issue in China. High PM_{2.5} concentrations can be
43 observed over eastern China from satellite observations (Xiao et al., 2020) and the PM_{2.5} concentrations
44 have been largely decreased since 2013 due to the effective control measures taken by the Chinese
45 government (Zhao et al., 2021). PM_{2.5} can affect air quality, ecosystems, and climate change and damage
46 human health through short-term or long-term exposure. The Global Burden of Disease study reported
47 that 1.1 million premature deaths were caused by long-term PM_{2.5} exposure over China in 2015 (Cohen
48 et al., 2017).

49 State-of-the-science three-dimensional air quality models (AQMs) have been widely used in China
50 as tools to simulate regional PM_{2.5} concentrations, quantify the contributions to total PM_{2.5} concentrations
51 resulting from emission sources and assess the benefits associated with control measures (Chang et al.;
52 2019, Li et al., 2015; Zhang et al., 2015; Zhang et al., 2019). The Weather Research and Forecasting
53 model-Community Multiscale Air Quality Modelling System (WRF-CMAQ) (Appel et al., 2017; Chang
54 et al., 2019), the Weather Research and Forecasting model coupled with Chemistry (WRF-Chem)
55 (Reddington et al., 2019), the Weather Research and Forecasting model-Comprehensive Air Quality
56 Model Extension (WRF-CAMx) (Li et al., 2015), and the Global Adjoint model of Atmospheric
57 Chemistry (GEOS-Chem Adjoint) (Zhang et al., 2015) were frequently used in previous studies. To
58 conduct a series of simulations for multiple scenarios or quantify the separate contributions attributable
59 to multiple sources, large computational resources and run-time are required while utilizing conventional
60 AQMs. To address these challenges and to improve the availability and accessibility of air quality
61 modelling, several reduced-complexity models have been developed by the air quality research

62 community. The three representative reduced-complexity air quality models frequently used are the
63 Estimating Air Pollution Social Impacts Using Regression (EASIUR) model (Heo et al., 2016; Heo et
64 al., 2017), the updated Air Pollution Emission Experiments and Policy (APEEP2) model (Muller et al.,
65 2007; Muller et al., 2011) and the Intervention for Air Pollution model (InMAP) (Tessum et al., 2017).
66 A recent study compares three reduced-complexity models, EASIUR, APEEP2, and InMAP, and the
67 results indicate that these three models are consistent in their assessment of the marginal social cost at
68 the county level (Gilmore et al., 2019). Reduced-complexity air quality models are less computationally
69 intensive and easier to use. However, it is not available in China. Therefore, it is essential to develop a
70 reduced-complexity air quality model over China to quickly predict $PM_{2.5}$ concentrations and the
71 associated health impacts of emission sources.

72 The reduced-complexity intervention model for air pollution, InMAP, was developed by Tessum et
73 al. (Tessum et al., 2017) to rapidly assess the air pollution, health, and economic impacts resulting from
74 marginal changes in air pollutant emissions. Compared with conventional air quality models, InMAP has
75 the advantage of being time-efficient, can predict annual-average $PM_{2.5}$ concentrations within a few
76 hours but with a modest reduction in accuracy compared with CTMs. InMAP reduces the running time
77 by simplifying the physical and chemical processes. InMAP has been used to assess marginal health
78 damage of location-specific emission sources (Goodkind et al., 2019), to quantify the health impacts of
79 individual coal-fired power plants in the United States (Thind et al., 2019), and to estimate the health
80 benefits of control policies considering specific locations (Sergi et al., 2020). However, to date, a version
81 of the reduced-complexity air quality intervention model over China is absent.

82 In this work, based on the source code of version 1.6.1 of InMAP model, a reduced-complexity air
83 quality intervention model over China (InMAP-China) is developed to rapidly predict the air quality and
84 estimate the health impacts of emission sources in China. The total consumed time for a simulation for
85 the year 2017 using the InMAP-China established in this study is approximately an hour with a single
86 CPU of 24 nodes. Therefore, it is convenient when conducting multiple simulations of $PM_{2.5}$
87 concentrations due to air pollutants emissions in 2017. The modelling system is applied over mainland
88 China for 2017 under various emission scenarios to examine model performance. Comparisons against
89 conventional air quality models and surface observations are performed in this study. The model
90 applicability and limitations are also declared.

91 The paper is organized as follows: Section 2.1 presents the components of InMAP-China including
92 the interface development between WRF-CMAQ and InMAP to generate parameters of the base

93 atmospheric state, the preprocessed process of emission input data, and the exposure-response functions
94 employed in this model. Section 2.2 introduces the evaluation protocol, including the statistical variables
95 adopted and the simulation design in this study. Section 3 presents the evaluation of InMAP-China's
96 predictions of PM_{2.5} air quality and PM_{2.5}-related health impacts in several simulations. Section 4
97 summarizes the conclusions and limitations of this study.

98 **2 Description of InMAP-China model**

99 **2.1 Model components and configurations**

100 The reduced-complexity intervention model for air pollution, InMAP, was developed by Tessum et
101 al. (Tessum et al., 2017) to rapidly assess the air pollution, health, and economic impacts resulting from
102 marginal changes in air pollutant emissions. The model has been widely used in studies (Sergi et al.,
103 2020; Thind et al., 2019; Goodkind et al., 2019; Dimanchevi et al., 2019) focusing on PM_{2.5} pollution
104 and health, economic impacts resulting from emission sources in the United States. In this model, the
105 continuous equation of atmospheric pollutants is solved at an annual scale, and the run time can be
106 reduced. The parameters used to represent physical and chemical processes for simplified simulation are
107 calculated before using CTM output data. PM_{2.5} air quality and PM_{2.5}-related premature mortality are
108 predicted and output in the InMAP model.

109 In this work, a Chinese version of the reduced-complexity air quality intervention model InMAP-
110 China is developed to rapidly estimate the PM_{2.5} concentration and associated health impacts of emission
111 sources. Figure 1 shows the model framework. Based on the source code of the InMAP model, three-
112 step development work is conducted to establish InMAP-China. First, we develop a preprocessed
113 interface to calculate physical and chemical process parameters using the WRF-CMAQ output variables
114 to support the simplified simulation in InMAP-China. Second, air pollutant emission data are
115 preprocessed to an appropriate format for the InMAP-China simulation. Third, the exposure-response
116 function of the GEMM model is employed in InMAP-China and replaces the original default function to
117 assess PM_{2.5}-related health impacts.

118 Table 1 presents the basic configurations of InMAP-China. The simulation domain is over East
119 Asia and covers mainland China. The spatial resolution is 36 km. Fourteen vertical layers are used in
120 InMAP-China, ranging from the surface layer to the top level of the tropospheric layer.

121 **2.1.1 Parameter interface development for simplified simulation in InMAP-China**

122 We develop a pre-processed interface to calculate physical and chemical process parameters using
123 WRF-CMAQ output variables for simplified simulation in InMAP-China based on the Environmental
124 Protection Agency's (EPA) work (Baker et al., 2020). Two NETCDF files containing the key parameters
125 for simplified simulation are generated by using the parameter interface developed here, one is at 36km
126 resolution across the entire mainland of China and another is at 4km resolution over the BTH region.
127 The main step of the pre-processed interface includes meteorological and chemical variable extraction
128 and merging, unit conversion, vertical layer mapping, physical and chemical process parameter
129 calculation, and average processing. The hourly chemical and meteorological variable outputs from the
130 WRF-CMAQ modelling system are converted into annual-average physical and chemical process
131 parameters required for simplified simulation.

132 A NetCDF file containing the three-dimensional annually-averaged parameters to characterize
133 atmospheric advection, dispersion, mixing, chemical reaction, and deposition is generated. Table 2 shows
134 the relationship between the annual-average parameters for simplified simulation and the original hourly
135 variables. In InMAP-China, the annual averaged component and the deviation of wind speed to represent
136 advection are calculated using hourly elements. The offset of wind vectors in different directions may
137 result in some uncertainties in this process. The parameters of eddy diffusion and convective transport
138 are pre-calculated using hourly elements, including temperature, pressure, boundary layer height, etc.
139 The annual wet deposition rate is determined by the rainwater mixing ratio and cloud fractions. The
140 annual dry deposition rate of particles and gaseous pollutants at the surface level is pre-calculated using
141 friction speed, heat flux, radiation flux, and land cover. The simplification of chemical reactions is
142 different among pollutants. For NO_x , NH_3 , and volatile organic compound (VOC) precursors, the annual
143 averaged gas-particle partitioning is adopted and calculated before using the output concentrations of
144 species from CMAQ. For SO_2 pollutants, the annual oxidation rate of two major conversion pathways
145 for SO_2 is calculated using concentrations of hydroxyl radical (HO) and hydrogen peroxide (H_2O_2) in
146 CMAQ, and the conversion is estimated in InMAP-China.

147 **2.1.2 Prior WRF-CMAQ simulation**

148 To generate the meteorological and chemical parameters required by InMAP-China, a one-year
149 WRF-CMAQ simulation covering the entire mainland of China is conducted to output hourly
150 meteorological and chemical-related variables in 2017. Besides, the nested WRF-CMAQ simulation over

151 the BTH region is also conducted and validated using observed data. The corresponded output data is
152 used to generate the meteorological and chemical parameters required by InMAP-China for the
153 simulations of 4 km resolution in the BTH region. Tables S1 and S2 show the major configurations of
154 the WRF-CMAQ modelling system. The WRF model is driven by the National Centers for
155 Environmental Prediction Final Analysis (NCEP-FNL) (<https://doi.org/10.5065/D6M043C6>) reanalysis
156 data to provide the initial and boundary conditions. The meteorological fields derived from the WRF
157 model is used to drive the CMAQ model (Appel et al., 2016) simulations. The air pollutant emissions
158 used here include anthropogenic emissions over China derived from the MEIC model
159 (<http://meicmodel.org/>), anthropogenic emissions over the region of East Asia outside China derived
160 from the MIX-2010 inventory (Li et al., 2015), and biogenic emissions derived from the MEGANv2.10
161 model. The CB05 chemical mechanism and the AERO6 aerosol module are employed in the model
162 simulation.

163 Table S3 summarizes the performance statistics of meteorological variables, including surface
164 temperature, relative humidity, and wind speed, in China in 2017, as simulated by the WRF model. The
165 hourly observed data of major meteorological variables derived from the National Climate Data Center
166 (NCDC) are utilized here. The results show that the meteorological variables simulated by the WRF
167 model agree well with the surface observations, which is consistent with previous studies (Wu et al.,
168 2019; Zheng et al., 2015; Hong et al., 2017). The model performs well on the predictions of surface
169 temperature, with an MB of -0.7 K, an NMB of -6.1%, and an R of 0.9. The predictions of relative
170 humidity at a height of 2 meters are relatively satisfied with an MB of 4.1% and an NMB of 6.1%. The
171 predictions of wind speed at a height of 10 meters are slightly overestimated, with an MB of 0.3 m/s and
172 an NMB of 12.4%, which may be caused by out-of-date USGS land use data employed in the model runs.

173 The SO₂, NO₂ and PM_{2.5} concentrations modelled across the domain agree well with the surface
174 observations in terms of the statistical performance and monthly variations. Table S4 summarizes the
175 performance of the statistics of major air pollutant concentrations. The nationwide annual averaged PM_{2.5}
176 concentration simulated in 2017 in China was 42.1 µg/m³. Compared with the observed PM_{2.5} of 45.9
177 µg/m³, there are slight underpredictions with an MB of 3.7 µg/m³ and NMB of 8.1%. The CMAQ model
178 has moderate underpredictions of the NO₂ concentrations and SO₂ concentrations, which may be related
179 to the uncertainties of emission inputs. For modelled NO₂ concentrations, MB and NMB are -4.6 µg/m³
180 and -13.9%, respectively. For modelled SO₂ concentrations, MB and NMB are -0.8 µg/m³ and -4.5%,

181 respectively. Figure S3 shows the monthly variation. The variation trend of the observed SO₂, NO₂, and
182 PM_{2.5} concentrations can be reproduced in the CMAQ simulations.

183 **2.1.3 Pre-processed emission input data**

184 We develop the pre-processed module to generate vector emission input for the InMAP-China
185 simulation. This module can allocate air pollutant emissions vertically and horizontally to supply the
186 missing parameters for the emission file and convert them into a shapefile vector format. The shapefile
187 vector format's emission data of 36km resolution in the entire mainland of China and 4km resolution in
188 the BTH region in 2017 are pre-processed by using this module.

189 In this module, the emission data are pre-processed by source and altitude. The anthropogenic
190 emissions of five sectors in China in 2017 from the MEIC inventory (<http://meicmodel.org/>), the
191 anthropogenic emissions over regions outside mainland China in Asia from the MIX-2010 inventory (Li
192 et al., 2015), and the natural emissions estimated using the MEGANv2.10 model (Guenther et al., 2012)
193 are employed in this study.

194 More detailed, the gridded anthropogenic emissions of 0.3 degrees for the residential, transportation,
195 and agricultural sectors are pre-processed and input to the surface layer. The gridded air pollutant
196 emissions of the industrial sector and non-coal power plants are pre-processed for allocation to attitudes
197 ranging from 130 meters to 240 meters and 130 meters to 890 meters, respectively. The emissions of
198 coal-fired power plants (CPPs) are pre-processed as point sources. The air pollutant emissions and the
199 stack attribution of each unit are provided in the emission file. Because the stack attribution of the power
200 unit is missed in the MEIC inventory, we supplied the information in the pre-processed module based on
201 NEI (National Emission Inventory data) data of power units. For stack height/stack diameter, a linear
202 relationship is first established (see Figure S1), and then, supplementation for these two parameters of
203 Chinese power plants is conducted by using the relationships. The fixed value for the other two variables
204 of stack attribution is set here because the PM_{2.5} concentrations attributable to power plants (CPPs-PM_{2.5})
205 are less sensitive to the two variables (see Figure S2). The stack gas exit velocity and stack gas exit
206 temperature of the power unit are 6 m/s and 313 K, respectively. The air pollutant emissions over regions
207 outside mainland China in Asia and the natural emissions simulated by MEGANv2.10 are pre-processed
208 and input to the surface layer.

209 **2.1.4 Exposure-response function from GEMM**

210 To rapidly estimate the premature mortality of PM_{2.5} exposures, we employ the exposure-response
211 function from GEMM to estimate PM_{2.5}-related premature mortality, which is developed by Burnett et
212 al. (Burnett et al., 2018), and calculate the premature mortality using PM_{2.5} concentration predictions of
213 InMAP-China. Premature mortality due to non-communicable diseases (NCDs) and lower respiratory
214 infections (LRIs) was considered in this study. Mortality is determined by the mortality incidence rate,
215 population, and attributable fraction (AF) to certain PM_{2.5} concentrations. The national mortality
216 incidence rate and the population data were derived from the GBD2017 study (Institute for Health
217 Metrics and Evaluation). The spatial distribution of the population in 2015 from the Gridded Population
218 of World Version 4 (Doxsey et al., 2015) was employed to allocate the population in 2017.

219 **2.2 Evaluation protocol**

220 **2.2.1 Evaluation method**

221 In this study, the performances of the InMAP-China predictions are evaluated by comparison
222 against CMAQ simulations and surface observations. Model-to-model comparison and model-to-
223 observation comparison have both been used to evaluate the performance of reduced-complexity air
224 quality models in previous studies (Tessum et al., 2017, Gilmore et al., 2019).

225 The following aspects are considered to make an evaluation. First, we examine the ability of
226 InMAP-China to predict PM_{2.5} concentrations at different emission levels, which will be introduced in
227 Section 3.1. Second, to examine the ability to quantify source contributions to PM_{2.5} concentrations, we
228 compare the InMAP-China's predictions of the sectoral contributions attributable to power, industry,
229 residential, transportation, and agriculture with those based on the CMAQ model, which will be
230 presented in Section 3.2. Third, to comprehensively understand the performance at higher spatial
231 resolution using InMAP-China, we compare the predictions of PM_{2.5} concentrations at 4km spatial
232 resolution in the BTH region both modelled by InMAP-China and conventional CMAQ with the
233 observations, which is displayed in Section 3.3. Fourth, focusing on the health impacts, the PM_{2.5}-related
234 premature mortality predicted by InMAP-China is also compared with mortality estimation based on
235 PM_{2.5} exposure derived from CMAQ, which is presented in Section 3.4.

236 For the observed PM_{2.5} concentration data, the annual averaged observed PM_{2.5} concentrations in
237 2017 were calculated using hourly concentration data from the China National Environmental
238 Monitoring Center, CNEMC (<http://www.cnemc.cn/>). More than 1400 national monitoring sites for air

239 pollutant concentrations are included in the simulation domain. The statistical parameters used in this
240 study include the correlation coefficient (R), mean bias (MB), mean error (ME), normalized mean bias
241 (NMB), normalized mean error (NME), and root mean square error (RMSE). The statistical analyses on
242 the performance of InMAP-China are similar to our previous evaluation of conventional CTMs (Zheng
243 et al., 2015; Wu et al., 2019).

244 **2.2.2 Experimental design**

245 We design twelve simulations to examine the model ability of InMAP-China in this study. Table 3
246 shows the sequence of simulations.

247 InMAP_TOT represents the baseline simulation with maximum emissions input, in which five
248 sectoral anthropogenic emissions are derived from the MEIC inventory, natural emissions are derived
249 from the MEGANv2.10 model, and Asian emissions outside mainland China are derived from the MIX-
250 2010 inventory are combined as emission inputs. Five sectoral and five abatement simulations are also
251 conducted to examine the ability of InMAP-China to predict concentration changes in response to
252 sectoral emissions and abatement emissions. The emission inputs for these ten simulations have been
253 declared in Table 3. The annual averaged physical and chemical process parameters are calculated based
254 on the output variables of WRF-CMAQ model, which has already been mentioned in Section 2.1.2.
255 Based on the above input, the particle continuity equations are solved by InMAP-China model to obtain
256 the annual averaged $PM_{2.5}$ concentrations at the steady-state of the atmosphere. The above simulations
257 are all conducted at 36km spatial resolution across the entire mainland of China. Besides, another
258 simulation represented by InMAP-BTH is conducted at 4km spatial resolution over the BTH region, with
259 the anthropogenic emission input data at 4km resolution derived from the MEIC inventory and natural
260 emissions derived from the MEGANv2.10 model is utilized in this simulation.

261 To make a comparison with the InMAP-China simulations, eleven CMAQ simulations are also
262 performed under the same emission inputs. The hourly $PM_{2.5}$ concentrations simulated by CMAQ in
263 2017 are averaged at obtaining the annual averaged $PM_{2.5}$ concentrations. Due to limited computational
264 resources, each simulation is conducted for four representative months (January, April, July, and October)
265 in 2017.

266 3 Results and Discussion

267 3.1 Model performance of PM_{2.5} concentrations in China

268 3.1.1 Total PM_{2.5} concentrations

269 Figure 3 shows the performance evaluation of total PM_{2.5} concentrations in the InMAP_TOT
270 simulations. Compared with the observed annual averaged PM_{2.5} concentrations, the total PM_{2.5}
271 concentrations are moderately underpredicted by InMAP-China with an MB of -8.1 μg/m³ and an NMB
272 of -18.1%. Compared with the CMAQ predictions, the total PM_{2.5} concentrations are also underpredicted,
273 with an MB of -5.3 μg/m³ due to the underprediction of primary PM_{2.5}. Consistent air pollutant emissions
274 are employed in the CMAQ and InMAP-China simulations. Therefore, the underpredictions are caused
275 by the different mechanisms in the two models. InMAP-China reproduces the spatial pattern of total
276 PM_{2.5} concentrations simulated by CMAQ. Notably, significant over predictions of PM_{2.5} concentrations
277 can be observed over mountain areas across Northern China, and the complex terrain and large emission
278 intensity increase the challenge of predicting PM_{2.5} concentrations using the reduced-complexity air
279 quality model in this region.

280 Figure 4 shows a comparison of PM_{2.5} compositions. Compared with the CMAQ results, the
281 InMAP-China predictions of PM_{2.5} compositions are satisfactory, with NMBs for SO₄²⁻, NO₃⁻, NH₄⁺, and
282 primary PM_{2.5} equal to 13%, -8%, -10%, and -23%, respectively. The predictions of SO₄²⁻, NO₃⁻, and
283 NH₄⁺ perform better than those of primary PM_{2.5}. Figure 5 and Figure 6 compare the spatial distribution
284 of PM_{2.5} compositions, and similar over-predictions of PM_{2.5} compositions can be observed in the
285 mountain area in Northern China.

286 The ability of InMAP-China to predict PM_{2.5} compositions is also examined at various emission
287 levels. Figure 7 compares the concentrations of PM_{2.5} compositions and the proportions of secondary
288 inorganic aerosols (hereafter, SNA) in total PM_{2.5} concentrations in different scenarios by two models.
289 In the InMAP_TOT scenario, the proportion of SNA is 56%, which is extremely close to the 50%
290 proportion in the WRF-CMAQ simulations. In five emission abatement simulations, the proportion was
291 approximately equal to that in the baseline scenario because the linearly treated chemical reaction
292 relationship of SNA was employed in InMAP-China. However, focusing on the simulations of five
293 sectoral emission scenarios, a significant difference can be observed, which is mainly caused by the
294 difference in chemical treatments in InMAP-China and CMAQ. In this situation, the impacts on PM_{2.5}
295 concentrations are distinct due to the nonlinear emission-concentration process.

296 3.1.2 Marginal change in PM_{2.5} concentrations

297 Figure 8 compares the InMAP-China and CMAQ predictions of population-weighted PM_{2.5}
298 concentrations and PM_{2.5} compositions for eleven emission scenarios. Marginal changes in air pollutant
299 concentrations are defined as 1 µg/m³ by normalizing the population-weighted air pollutant
300 concentrations of each scenario using the largest value among all scenarios modelled by CMAQ. The
301 InMAP-China reproduces CMAQ predictions on the marginal change in population-weighted PM_{2.5}
302 concentrations, with an NMB of -12% and correlations of 0.98, as shown in Figure 8(a). This
303 performance is similar to that predicted by InMAP in the United States (Tessum et al., 2017).

304 Figure 8(b)-(f) compares the predictions of PM_{2.5} compositions. The InMAP-China predictions of
305 SO₄²⁻, NO₃⁻, NH₄⁺ and primary PM_{2.5} agree well with the CMAQ results, but the predictions of secondary
306 organic aerosol (SOA) are the poorest. The marginal changes in NO₃⁻ and primary PM_{2.5} concentrations
307 are moderately underpredicted by InMAP-China, with an NMB value of -13% and -21%, respectively.
308 Conversely, the marginal change in SO₄²⁻ concentrations are over-predicted with an NMB of 23%. The
309 marginal change in NH₄⁺ predicted by InMAP-China agrees well with the CMAQ predictions. Because
310 few reaction pathways of SOA are included in the CB05 mechanism in the CMAQ simulations, SOAs
311 are under-predicted in the entire modelling system.

312 The regional performance of the changes in PM_{2.5} and its compositions for eleven emission
313 scenarios is also examined in this study. Figures S4-S7 show the regional results. Four regions, including
314 the Beijing-Tianjin-Hebei region (BTH), Yangtze River Delta (YRD), Pearl River Delta (PRD), and
315 Fen Wei Plain (FWP), are analyzed here (see Figure 2). At the regional level, the CMAQ predicted
316 marginal changes in population-weighted PM_{2.5} concentrations, and its composition can be reproduced
317 by InMAP-China, which is similar to the nationwide performance. However, the marginal change in
318 SO₄²⁻ concentrations over the BTH is significantly over-predicted by InMAP-China, with an NMB of
319 135%, which is expected to be improved by optimizing the representation of the annual sulfate oxidation
320 rate in this region.

321 3.2 Model performance of source contributions in China

322 Figure 9 shows the contribution of each sector to PM_{2.5} concentrations nationwide and at the regional
323 scale, and Table 4 displays the proportion value of sectoral contribution based on two models. The
324 predictions of the source contributions of PM_{2.5} concentrations in InMAP-China are reliable compared
325 with those based on the CMAQ model, and the difference can be explained.

326 The results based on the two models indicate that the industrial and residential sectors are the first
327 and second contributors among the five sectors. The contribution of the electricity sector is comparable
328 when using the two models, while the contributions of transportation and agriculture are moderately
329 different, which is mainly due to the difference in the model mechanism and the treatment of secondary
330 inorganic aerosols in the two models. At the regional scale, the difference in the sectoral contribution
331 caused by the mechanism in the two models is more significant than at the national scale.

332 **3.3 Model performance of PM_{2.5} predictions at higher resolution in the BTH region**

333 We also conducted a simulation with a higher spatial resolution of 4 km in the BTH region by using
334 InMAP-China model and make a comparison with the WRF-CMAQ nested simulation at the same area
335 in the BTH region. Figure 10 and Figure 11 show the performance evaluation of total PM_{2.5} concentration
336 and the composition in the InMAP_BTH scenario. Compared with the observed annual averaged PM_{2.5}
337 concentrations, the total PM_{2.5} concentrations are moderately overpredicted in InMAP_BTH with an
338 NMB of 41.3% and an R of 0.5.

339 Further compared with the nested CMAQ predictions, the total PM_{2.5} concentrations are also over-
340 predicted by InMAP-China model. The predictions of PM_{2.5} compositions in the InMAP_BTH scenario
341 are partially satisfactory, except for SO₄²⁻, with NMBs for SO₄²⁻, NO₃⁻, NH₄⁺, and primary PM_{2.5} equal
342 to 178%, 36%, 33%, and 27%, respectively. Figure 12 further shows the comparison of the spatial
343 distribution of PM_{2.5} compositions in the BTH region. The overall spatial distribution pattern of PM_{2.5}
344 compositions is similarly modeled by two models, however, an obvious difference can be observed
345 across the mountain area in the BTH region, for instance, the over-predictions of PM_{2.5} compositions,
346 especially, SO₄²⁻ and NO₃⁻ observed near the Taihang mountain area.

347 **3.4 Model performance of PM_{2.5}-related premature mortality in China**

348 To examine the performance of the predictions of PM_{2.5}-related premature mortality, a comparison
349 of premature mortality using the PM_{2.5} predictions from InMAP-China and CMAQ, separately, is
350 performed here. Figure 13 shows the comparison based on two models for all provinces. The results
351 demonstrate that, compared with the premature mortality based on CMAQ, the relative difference is
352 ranging from -44% to 15% at the provincial level due to the difference of PM_{2.5} concentrations in the two
353 models.

354 At the provincial level, the PM_{2.5}-related premature mortality in Beijing city, Tianjin city, Hebei
355 province, and Shanghai city is slightly over-predicted by InMAP-China, with the relative difference

356 ranging from 4% to 15%. Conversely, for the other majority of provinces, PM_{2.5}-related premature
357 mortality is under-predicted by InMAP-China, with the relative difference ranging from -3% to -44%.
358 Overall, the PM_{2.5}-related premature mortality estimated using InMAP-China was 1.92 million people in
359 2017. Compared with the CMAQ-based estimations, 25 ten thousand deaths are under-predicted by
360 InMAP-China because of underestimation of total PM_{2.5} concentrations in the baseline simulation.

361 **4 Conclusions**

362 This work develops a reduced-complexity air quality intervention model over China and presents a
363 comprehensive evaluation by comparing CMAQ simulations and surface observations. The InMAP-
364 China aims at providing a simplified modelling tool to rapidly predict the PM_{2.5} concentrations due to
365 emission change as well as the health impact of emission sources in China. After the model is established,
366 the total consumed time for a new simulation under the atmosphere condition in the year 2017 across the
367 mainland of China using InMAP-China is merely an hour with a single CPU of 24 nodes. Therefore, it
368 is time-efficient when conducting new simulations of PM_{2.5} concentrations in China. Notably, the
369 running of WRF-CMAQ simulations is merely necessary for our developing stage of InMAP-China. For
370 the application of InMAP-China, we recommend users to select InMAP-China as a prior tool with
371 extensive simulation demands, for instance, to quantify the PM_{2.5} concentrations due to hundreds of
372 pollution emitters or to rapidly estimate the PM_{2.5} concentrations caused by dozens of control policies,
373 separately. Besides, the variable grid can also be set in InMAP-China to allow a high spatial resolution
374 of 1km or even higher in a certain urban area.

375 InMAP-China has moderately satisfactory performance in this study, however, this model has
376 reductions in accuracy compared with conventional CTMs. Overall, InMAP-China satisfactorily predicts
377 total PM_{2.5} concentrations in the baseline simulation in terms of statistical performance. Compared with
378 the observed PM_{2.5} concentrations, the MB, NMB, and correlations of the total PM_{2.5} concentrations are
379 -8.1 µg/m³, -18%, and 0.6, respectively. The statistical performance is satisfactory for a reduced-
380 complexity air quality model and remains consistent with the performance evaluation in the United States.
381 The underestimation of total PM_{2.5} mainly comes from the primary PM_{2.5}. Moreover, the spatial pattern
382 of total PM_{2.5} concentrations can be reproduced in InMAP-China, while an overestimation over the
383 mountain area in Northern China can be observed. The large emission intensity and complex terrain over
384 this region increase the difficulty of modelling concentrations in this area. The predictions of source
385 contributions to PM_{2.5} concentrations by InMAP-China are comparable with those based on the CMAQ

386 model, and the difference is mainly caused by the uncertainty of the simplification of the chemical
387 process in the InMAP-China. The global version of the reduced-complexity air quality model (Global-
388 InMAP) is also developed and released recently (Thakrar et al., 2021), our results of InMAP-China can
389 provide more accurate results in the mainland of China.

390 This study is subject to some limitations and uncertainties. In InMAP-China, the annual-average
391 chemical and physical processes parameters are calculated using hourly parameters from WRF-CMAQ.
392 Complicated seasonal and daily variations affecting the formation and transportation of particulate matter
393 are challenging to retain. The intensity of advection of the air mass is supposed to be weakened due to
394 the offset of the wind vector in the averaging process, which was also pointed out in a previous study.
395 Moreover, InMAP-China has difficulty predicting SOA concentrations because reaction pathways for
396 SOA are insufficient in this modelling system. Further research work is suggested to improve the model
397 performance. For instance, the combination of machine learning with the simplified simulation may need
398 to research to promote the reduced-complexity air quality modeling over China.

399

400

401

402

403

404

405

406

407

408

409

410

411

412

413

414

415 **Code and data availability**

416 The source code for the localized version of the reduced-complexity air quality model over China
417 (InMAP-China), which is developed based on the original InMAP model over the United States. The
418 data related to this study as well as the user manual are available at
419 <https://doi.org/10.5281/zenodo.5111961>.

420 **Author contributions**

421 Q. Zhang and RL. Wu designed the research and RL. Wu carried them out. RL. Wu, CW. Tessum and
422 Y. Zhang contributed to model development. R. L. Wu and Q. Zhang interpreted the results. RL. Wu
423 prepared the manuscript with contributions from all co-authors.

424 **Competing interests**

425 The authors declare no competing interests.

426 **Acknowledgements**

427 This work was supported by the National Natural Science Foundation of China (41625020 and
428 41921005). And this work was also funded under Assistance Agreement No. RD835871 awarded by the
429 U.S. EPA to Yale University. The views expressed in this manuscript are those of the authors alone and
430 do not necessarily reflect the views and policies of the U.S. EPA. The EPA does not endorse any products
431 or commercial services mentioned in this publication.

432
433
434
435
436
437
438
439
440
441

442 **References**

- 443 Appel, K.W., Napelenok, S.L., Hogrefe, C., Foley, K.M., Pouliot, G.A., Murphy, B., Heath, N., Roselle,
444 S., Pleim, J., Bash, J.O., Pye, H.O.T., Mathur, R. Overview and evaluation of the Community Multiscale
445 Air Quality (CMAQ) modelling system version 5.2. *Air Pollution Modelling and its Application XXV*,
446 11:63-72. ITM 2016. Springer Proceedings in Complexity. Springer, Cham, doi: 10.1007/978-3-319-
447 57645-9_11, 2017.
- 448 Appel, K.W., Napelenok, S.L., Hogrefe, C., Foley, K.M., Pouliot, G.A., Murphy, B., Heath, N., Roselle,
449 S., Pleim, J., Bash, J.O., Pye, H.O.T., Mathur, R. Overview and evaluation of the Community Multiscale
450 Air Quality (CMAQ) modelling system version 5.2. *Air Pollution Modelling and its Application XXV*,
451 11:63-72. ITM 2016. Springer Proceedings in Complexity. Springer, Cham, doi: 10.1007/978-3-319-
452 57645-9_11, 2017.
- 453 Baker, K. R.; Amend, M.; Penn, S.; Bankert, J.; Simon, H.; Chan, E.; Fann, N.; Zawacki, M.; Davidson,
454 K.; Roman, H., A database for evaluating the InMAP, APEEP, and EASIUR reduced complexity air-
455 quality modelling tools. *Data in Brief*, 28, 2020.
- 456 Burnett, R.; Chen, H.; Szyszkowicz, M.; Fann, N.; Hubbell, B.; Pope, C. A.; Apte, J. S.; Brauer, M.;
457 Cohen, A.; Weichenthal, S.; Coggins, J.; Di, Q.; Brunekreef, B.; Frostad, J.; Lim, S. S.; Kan, H. D.;
458 Walker, K. D.; Thurston, G. D.; Hayes, R. B.; Lim, C. C.; Turner, M. C.; Jerrett, M.; Krewski, D.; Gapstur,
459 S. M.; Diver, W. R.; Ostro, B.; Goldberg, D.; Crouse, D. L.; Martin, R. V.; Peters, P.; Pinault, L.;
460 Tjepkema, M.; Donkelaar, A.; Villeneuve, P. J.; Miller, A. B.; Yin, P.; Zhou, M. G.; Wang, L. J.; Janssen,
461 N. A. H.; Marra, M.; Atkinson, R. W.; Tsang, H.; Thach, Q.; Cannon, J. B.; Allen, R. T.; Hart, J. E.;
462 Laden, F.; Cesaroni, G.; Forastiere, F.; Weinmayr, G.; Jaensch, A.; Nagel, G.; Concin, H.; Spadaro, J.
463 V., Global estimates of mortality associated with long-term exposure to outdoor fine particulate matter.
464 *Proceedings of the National Academy of Sciences of the United States of America*, 115, (38), 9592-9597,
465 2018.
- 466 C. J. Walcek, Taylor GR. A Theoretical Method for Computing Vertical Distributions of Acidity and
467 Sulfate Production within Cumulus Clouds. *Journal of the Atmospheric Science*, 43:339-55, 1986.
- 468 Chang, X.; Wang, S.; Zhao, B.; Xing, J.; Liu, X.; Wei, L.; Song, Y.; Wu, W.; Cai, S.; Zheng, H.; Ding,
469 D.; Zheng, M., Contributions of inter-city and regional transport to PM_{2.5} concentrations in the Beijing-

470 Tianjin-Hebei region and its implications on regional joint air pollution control. *Science of the Total*
471 *Environment*, 660, 1191-1200, 2019.

472 Cohen, A. J.; Brauer, M.; Burnett, R.; Anderson, H. R.; Frostad, J.; Estep, K.; Balakrishnan, K.;
473 Brunekreef, B.; Dandona, L.; Dandona, R.; Feigin, V.; Freedman, G.; Hubbell, B.; Jobling, A.; Kan, H.;
474 Knibbs, L.; Liu, Y.; Martin, R.; Morawska, L.; Pope, C. A., III; Shin, H.; Straif, K.; Shaddick, G.; Thomas,
475 M.; van Dingenen, R.; van Donkelaar, A.; Vos, T.; Murray, C. J. L.; Forouzanfar, M. H., Estimates and
476 25-year trends of the global burden of disease attributable to ambient air pollution: an analysis of data
477 from the Global Burden of Diseases Study 2015. *Lancet* 389, (10082), 1907-1918, 2017.

478 Dimanchevi, E. G.; Paltsev, S.; Yuan, M.; Rothenberg, D.; Tessum, C. W.; Marshall, J. D.; Selin, N. E.,
479 Health co-benefits of sub-national renewable energy policy in the US. *Environmental Research Letters*,
480 14, (8) ,2019.

481 Doxsey-Whitfield E, MacManus K, Adamo S B, Susana B, Pistolesi L, Squires J, Borkovska O and
482 Baptista S R Taking advantage of the improved availability of census data: a first look at the gridded
483 population of the world, version 4. *Papers in Applied Geography*. 1 226–34, 2015.

484 E. J. Mlawer, S. J. Taubman, P. D. Brown, M. J. Iacono, S. A. Clough. Radiative transfer for
485 inhomogeneous atmospheres: RRTM, a validated correlated-k model for the longwave. *Journal of*
486 *Geophysical Research*, 102:16663-82, 1997.

487 Fountoukis C and Nenes A. ISORROPIA II: A Computationally Efficient Aerosol Thermodynamic
488 Equilibrium Model for K^+ , Ca^{2+} , Mg^{2+} , NH_4^+ , Na^+ , SO_4^{2-} , NO_3^- , Cl^- , H_2O Aerosols, *Atmospheric*
489 *Chemistry Physics*, 7, 4639-4659, 2007.

490 Gilmore, E. A.; Heo, J.; Muller, N. Z.; Tessum, C. W.; Hill, J. D.; Marshall, J. D.; Adams, P. J., An inter-
491 comparison of the social costs of air quality from reduced-complexity models. *Environmental Research*
492 *Letters*, 14, (7), 2019.

493 Global Burden of Disease Collaborative Network. *Global Burden of Disease Study 2017 (GBD 2017)*
494 *Population Estimates 1950-2017*. Seattle, United States: Institute for Health Metrics and Evaluation
495 (IHME), 2018.

496 Global Burden of Disease Collaborative Network. Global Burden of Disease Study 2017 (GBD 2017)
497 Cause-Specific Mortality 1980-2017. Seattle, United States: Institute for Health Metrics and Evaluation
498 (IHME), 2018.

499 Goodkind AL, Tessum CW, Coggins JS, Hill JD, Marshall JD. Fine-scale damage estimates of particulate
500 matter air pollution reveal opportunities for location-specific mitigation of emissions. Proceedings of the
501 National Academy of Sciences. Apr 3:201816102. <https://doi.org/10.1073/pnas.1816102116>, 2019.

502 Guenther, A. B.; Jiang, X.; Heald, C. L.; Sakulyanontvittaya, T.; Duhl, T.; Emmons, L. K.; Wang, X.,
503 The Model of Emissions of Gases and Aerosols from Nature version 2.1 (MEGAN2.1): an extended and
504 updated framework for modelling biogenic emissions. Geoscientific Model Development Discussions,
505 5, (2), 1503-1560, 2012.

506 Heo, J.; Adams, P. J.; Gao, H. O., Public health costs accounting of inorganic PM_{2.5} pollution in
507 metropolitan areas of the United States using a risk-based source-receptor model. Environment
508 International, 106, 119-126, 2017.

509 Heo, J.; Adams, P. J.; Gao, H. O., Reduced-form modelling of public health impacts of inorganic PM_{2.5}
510 and precursor emissions. Atmospheric Environment, 137, 80-89, 2016.

511 Hong, C.; Zhang, Q.; Zhang, Y.; Tang, Y.; Tong, D.; He, K., Multi-year downscaling application of two-
512 way coupled WRF v3.4 and CMAQ v5.0.2 over east Asia for regional climate and air quality modelling:
513 model evaluation and aerosol direct effects. Geoscientific Model Development, 10, (6), 2447-2470, 2017.

514 J. E. Pleim. A Combined Local and Nonlocal Closure Model for the Atmospheric Boundary Layer. Part
515 I: Model Description and Testing. Journal of Applied Meteorology and Climatology, 46:1383-95, 2007.

516 J. S. Chang, R. A. Brost, I. S. A. Isaksen, S. Madronich, P. Middleton, W. R. Stockwell, et al. A three-
517 dimensional Eulerian acid deposition model: Physical concepts and formulation. Journal of Geophysical
518 Research, 92:14681-700, 1987.

519 J. S. Kain. The Kain–Fritsch Convective Parameterization: An Update. Journal of Applied Meteorology.
520 2004, 43:170-81.

521 Li, M.; Zhang, Q.; Kurokawa, J.-i.; Woo, J.-H.; He, K.; Lu, Z.; Ohara, T.; Song, Y.; Streets, D. G.;
522 Carmichael, G. R.; Cheng, Y.; Hong, C.; Huo, H.; Jiang, X.; Kang, S.; Liu, F.; Su, H.; Zheng, B., MIX:
523 a mosaic Asian anthropogenic emission inventory under the international collaboration framework of the

524 MICS-Asia and HTAP. *Atmospheric Chemistry and Physics*, 17, (2), 935-963, 2017.

525 Li, X.; Zhang, Q.; Zhang, Y.; Zheng, B.; Wang, K.; Chen, Y.; Wallington, T. J.; Han, W.; Shen, W.; Zhang,
526 X.; He, K., Source contributions of urban PM_{2.5} in the Beijing-Tianjin-Hebei region: Changes between
527 2006 and 2013 and relative impacts of emissions and meteorology. *Atmospheric Environment*, 123, 229-
528 239, 2015.

529 Liu, F.; Zhang, Q.; Tong, D.; Zheng, B.; Li, M.; Huo, H.; He, K. B., High-resolution inventory of
530 technologies, activities, and emissions of coal-fired power plants in China from 1990 to 2010.
531 *Atmospheric Chemistry and Physics*, 15, (23), 13299-13317, 2015.

532 M.-D. Chou, M. J. Suarez, C.-H. Ho, M. M.-H. Yan, K.-T. Lee. Parameterizations for Cloud Overlapping
533 and Shortwave Single-Scattering Properties for Use in General Circulation and Cloud Ensemble Models.
534 *Journal of Climate*, 11:202-14, 1998.

535 Muller, N. Z., Mendelsohn, R. Measuring the damages of air pollution in the United States. *Journal of*
536 *Environmental Economics and Management*, 54(1), 1–14. <https://doi.org/10.1016/j.jeem.2006.12.002>,

537 Muller, N. Z., Mendelsohn, R., & Nordhaus, W. Environmental accounting for pollution in the United
538 States economy. *American Economic Review*, 101(5), 1649-75. DOI:10.1257/aer.101.5.1649, 2011.

539 Multi-resolution Emission Inventory of China (<http://meicmodel.org/>).

540 National Centers for Environmental Prediction/National Weather Service/NOAA/US Department of
541 Commerce NCEP FNL Operational Model Global Tropospheric Analyses, continuing from July 1999
542 Dataset (<https://doi.org/10.5065/D6M043C6>), 2000.

543 Reddington, C. L.; Conibear, L.; Knote, C.; Silver, B.; Li, Y. J.; Chan, C. K.; Arnold, S. R.; Spracklen,
544 D. V., Exploring the impacts of anthropogenic emission sectors on PM_{2.5} and human health in South and
545 East Asia. *Atmospheric Chemistry and Physics*, 19, (18), 11887-11910, 2019.

546 Sergi, B. J.; Adams, P. J.; Muller, N. Z.; Robinson, A. L.; Davis, S. J.; Marshall, J. D.; Azevedo, I. L.,
547 Optimizing Emissions Reductions from the U.S. Power Sector for Climate and Health Benefits.
548 *Environmental science & technology*, 54, (12), 7513-7523, 2020.

549 Skamarock W, Klemp J, Dudhia J, Gill D, Barker D, Duda M, Huang X, Wang J, Powers J A
550 description of the Advanced Research WRF Version 3 NCAR technical note (Boulder, CO: National
551 Center for Atmospheric Research), 2008.

552 Tessum, C. W.; Hill, J. D.; Marshall, J. D., InMAP: A model for air pollution interventions. PLoS One,
553 12, (4), e0176131, 2017.

554 Thakrar S. T.; Tessum C. W.; Apte J. S.; Balasubramanian S; Millet D. B.; Pandis S. N.; Marshall J. D.;
555 Hill J. D., et al. Global, High-Resolution, Reduced-Complexity Air Quality Modeling Using InMAP
556 (Intervention Model for Air Pollution). Earth, Space and Environmental Chemistry (preprinted), 2021.

557 Thind, M. P. S.; Tessum, C. W.; Azevedo, I. L.; Marshall, J. D., Fine Particulate Air Pollution from
558 Electricity Generation in the US: Health Impacts by Race, Income, and Geography. Environmental
559 Science & Technology, 53, (23), 14010-14019, 2019.

560 United States Environmental Protection Agency. National Emission Inventory data.
561 <https://www.epa.gov/air-emissions-inventories/2011-national-emissions-inventory-nei-data>. 2011.

562 Whitten G Z, Heo G, Kimura Y, et al. A new condensed toluene mechanism for Carbon Bond CB05-TU.
563 Atmospheric Environment, 44(40SI):5346-5355, 2010.

564 Wu, R.; Liu, F.; Tong, D.; Zheng, Y.; Lei, Y.; Hong, C.; Li, M.; Liu, J.; Zheng, B.; Bo, Y.; Chen, X.; Li,
565 X.; Zhang, Q., Air quality and health benefits of China's emission control policies on coal-fired power
566 plants during 2005–2020. Environmental Research Letters, 14, (9), 094016, 2019.

567 Xiao, Q. Y.; Geng, G. N.; Liang, F. C.; Wang, X.; Lv, Z.; Lei, Y.; Huang, X. M.; Zhang, Q.; Liu, Y.; He,
568 K., Changes in spatial patterns of PM_{2.5} pollution in China 2000–2018: Impact of clean air policies.
569 Environment international, 141, 105776, 2020.

570 Xiu, A., Pleim, J. E., Development of a Land Surface Model. Part I: Application in a Mesoscale
571 Meteorological Model. Journal of Applied Meteorology, 40:192-209, 2011.

572 Zhang, L.; Liu, L. C.; Zhao, Y. H.; Gong, S. L.; Zhang, X. Y.; Henze, D. K.; Capps, S. L.; Fu, T. M.;
573 Zhang, Q.; Wang, Y. X., Source attribution of particulate matter pollution over North China with the
574 adjoint method. Environmental Research Letters, 10, (8), 2015.

575 Zhang, Q.; Zheng, Y.; Tong, D.; Shao, M.; Wang, S.; Zhang, Y.; Xu, X.; Wang, J.; He, H.; Liu, W.; Ding,
576 Y.; Lei, Y.; Li, J.; Wang, Z.; Zhang, X.; Wang, Y.; Cheng, J.; Liu, Y.; Shi, Q.; Yan, L.; Geng, G.; Hong,
577 C.; Li, M.; Liu, F.; Zheng, B.; Cao, J.; Ding, A.; Gao, J.; Fu, Q.; Huo, J.; Liu, B.; Liu, Z.; Yang, F.; He,
578 K.; Hao, J., Drivers of improved PM_{2.5} air quality in China from 2013 to 2017. Proceedings of the
579 National Academy of Sciences of the United States of America, 116, (49), 24463-24469, 2019.

580 Zheng, B.; Zhang, Q.; Zhang, Y.; He, K. B.; Wang, K.; Zheng, G. J.; Duan, F. K.; Ma, Y. L.; Kimoto, T.,
581 Heterogeneous chemistry: a mechanism missing in current models to explain secondary inorganic aerosol
582 formation during the January 2013 haze episode in North China. *Atmospheric Chemistry and Physics*,
583 15, (4), 2031-2049, 2015.

584

585

586

587

588

589

590

591

592

593

594

595

596

597

598

599

600

601

602

603

604

605

606

607

608 **Table 1. Model configurations in InMAP-China.**

Category	Parameters	Configurations
Basic	Research area and period	China, 2017
	Spatial resolution	36 km × 36 km
	Vertical layers	14 layers
	Run type	Steady run
	Variable grid	Static grid
	Projection	Lambert
	Grid numbers	305816
Input	Meteorological and chemical parameters	Calculated using variables from WRFv3.8-CMAQv5.2
	Anthropogenic emissions	MEIC, MIX, MEGAN
	Population data	GPW 2015 and GBD 2017
	Baseline mortality rate	GBD 2017
Output	Air pollutants	PM _{2.5} and its composition concentrations
	Mortality	PM _{2.5} -related premature mortality

609

610

611

612

613

614

615

616

617

618

Table 2 The relationship between parameters for simplified simulation and original variables.

WRF-CMAQ's Variables	Descriptions	InMAP-China's Parameters	Descriptions
U, V, W	Wind fields	UAvg, UDeviation VAvg, VDeviation WAvg, WDeviation	Advection and mixing coefficients
PH, PHB	Base state of geopotential and perturbation geopotential	Dz	Layer heights
PBLH	Planetary boundary layer height	M2d, M2u, Kxxyy, Kzz	Mixing coefficients
T	Potential Temperature	SO ₂ Oxidation, PlumeHeight	Chemical reaction rates and plume rise
P, PB	Base state pressure plus perturbation pressure		Chemical reaction rates and plume rise
QRAIN	Mixing ratio of rain	ParticleWetdep, GasWetdep	Wet deposition
QCLOUD	Cloud mixing ratio	SO ₂ Oxidation	Aqueous-phase chemical reaction rates
CLDFRA	Fraction of grid cell covered by clouds	ParticleWetdep, GasWetdep	Wet deposition
SWDOW N, GLW	Downward shortwave and longwave radiative flux at ground level	GasDrydep, ParticleWetdep	Dry deposition
HFX	Surface heat flux	M2d, M2u, Kxxyy, Kzz, Drydep	Mixing and dry deposition
UST	Friction velocity		Mixing and dry deposition
LU_INDE X	Land use type	M2d, M2u, Kxxyy, Kzz	Mixing
DENS	Inverse air density		Mixing and convert between mixing ratio and mass concentration
aVOC	Anthropogenic VOCs that are SOA precursors	aOrgPartitioning	VOCs/SOA partitioning
aSOA	Anthropogenic SOA		
OH, H ₂ O ₂	Hydroxyl radical and hydrogen peroxide concentrations	SO ₂ Oxidation	Oxidation rates
pNO	ANO ₃ I, ANO ₃ J	NOPartitioning	

gNO	NO and NO ₂		NO _x /pNO ₃ partitioning
pNH	ANH ₄ I, ANH ₄ J	NHPartitioning	NH ₃ /pNH ₄ partitioning
gNH	NH ₃		

620
621
622
623
624
625
626
627
628
629
630
631
632
633
634
635
636
637
638
639
640
641
642
643

644 **Table 3 Simulation experiments conducted using InMAP-China.**

Class	Simulations	Emission input	Physical and chemical parameter input
Base	InMAP_TOT	Five sectoral anthropogenic emissions and natural emissions	
High_re	InMAP_BTH	Five sectoral anthropogenic emissions and natural emissions with 4km resolution at BTH region	
Sec1	InMAP_POW	Power plants emissions	
Sec2	InMAP_INDUS	Industrial emissions	
Sec3	InMAP_TRANS	Transportation emissions	
Sec4	InMAP_RESI	Residential emissions	
Sec5	InMAP_AGRI	Agricultural emissions	
Aba1	InMAP_RE10	Reduce the air pollutants emissions by 10% based on InMAP_TOT emissions	
Aba2	InMAP_RE30	Reduce the air pollutants emissions by 30% based on InMAP_TOT emissions	Converted using WRF-CMAQv5.2 simulation data in the year of 2017;
Aba3	InMAP_RE50	Reduce the air pollutants emissions by 50% based on InMAP_TOT emissions	Remain the same in all simulations.
Aba4	InMAP_RE70	Reduce the air pollutants emissions by 70% based on InMAP_TOT emissions	
Aba5	InMAP_RE90	Reduce the air pollutants emissions by 90% based on InMAP_TOT emissions	

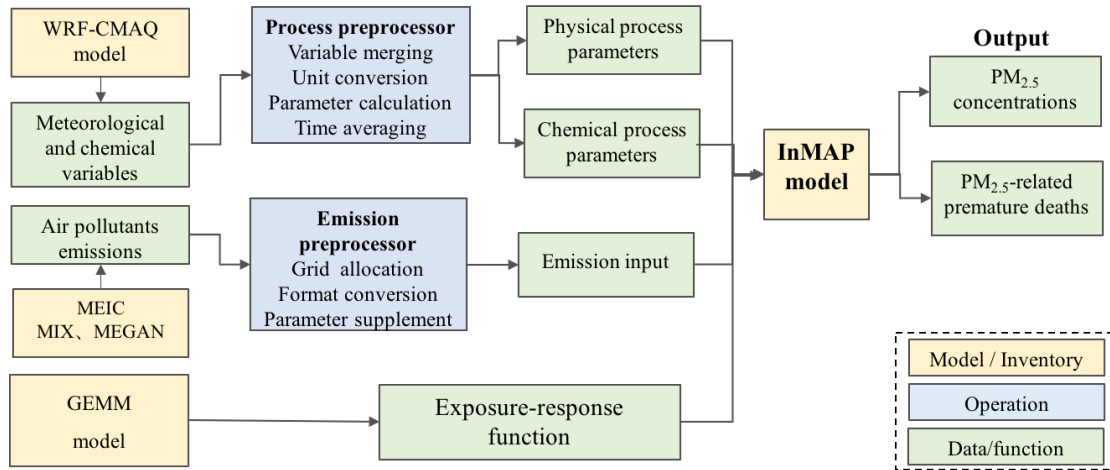
645
646
647
648
649
650
651
652

653 **Table 4 Comparison of the proportions of sectoral contributions to PM_{2.5} concentrations using InMAP-**
 654 **China and CMAQ.**

Sector	National		BTH		YRD		PRD		FWPY	
	CMAQ	InMAP- P- China	CMAQ	InMAP- P- China	CMAQ	InMAP- P- China	CMAQ	InMAP- P- China	CMAQ	InMAP- P- China
Power	6.9%	8.1%	6.2%	9.4%	7.4%	8.6%	10.4%	8.2%	7.0%	10.0%
Industry	30.8%	35.0%	30.2%	38.2%	33.3%	39.1%	37.5%	35.4%	27.7%	31.9%
Residential	25.9%	28.1%	24.7%	28.2%	17.9%	20.8%	19.5%	28.4%	30.0%	33.8%
Transportation	14.0%	17.3%	13.4%	15.6%	15.7%	21.2%	17.1%	17.5%	13.2%	15.0%
Agriculture	22.5%	11.5%	25.5%	10.4%	25.7%	12.4%	15.4%	11.6%	22.0%	9.4%

655
 656
 657
 658
 659
 660
 661
 662
 663
 664
 665
 666
 667

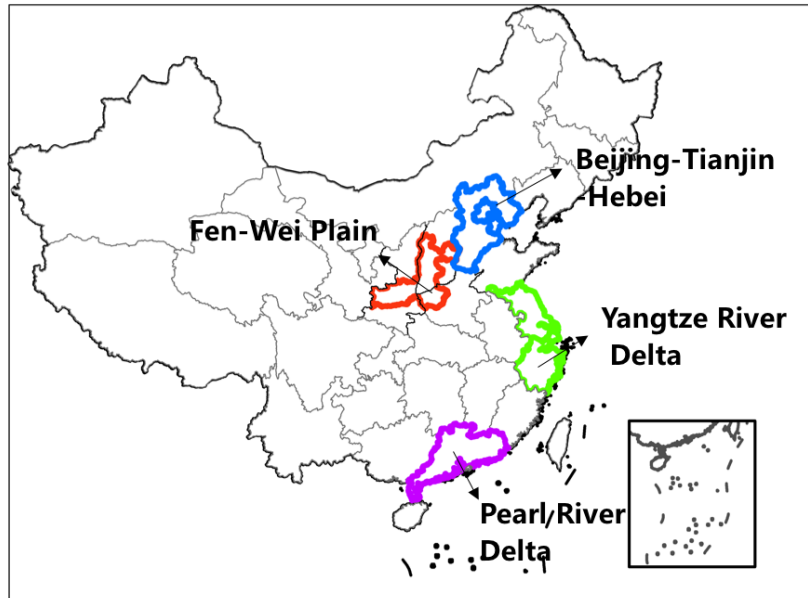
InMAP-China model



668
669

670 **Figure 1 Model framework of InMAP-China.**

671
672
673
674
675
676
677
678
679
680
681
682
683
684



685

686

687 **Figure 2** Four key regions are defined in this study, including the Beijing-Tianjin-Hebei region, Yangtze River
688 **Delta region, Pearl River Delta region, and Fen Wei Plain region.**

689

690

691

692

693

694

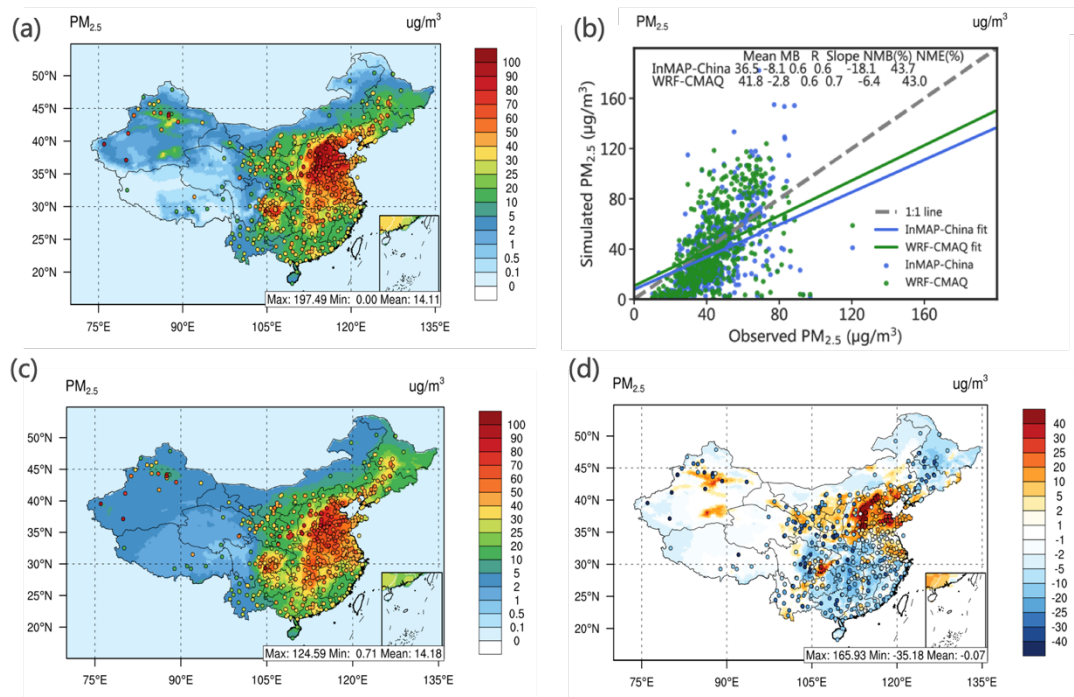
695

696

697

698

699



700

701

Figure 3 The spatial pattern and statistical metrics of total PM_{2.5} concentrations predicted by InMAP-China

702

and WRF-CMAQ. Panels (a) and (c) display the spatial patterns of total PM_{2.5} concentrations predicted by InMAP-

703

China and WRF-CMAQ, respectively. Panel (d) presents the difference in the spatial distribution of the total PM_{2.5}

704

concentrations predicted by the two models. Panel (b) shows the statistical metrics between the simulated and

705

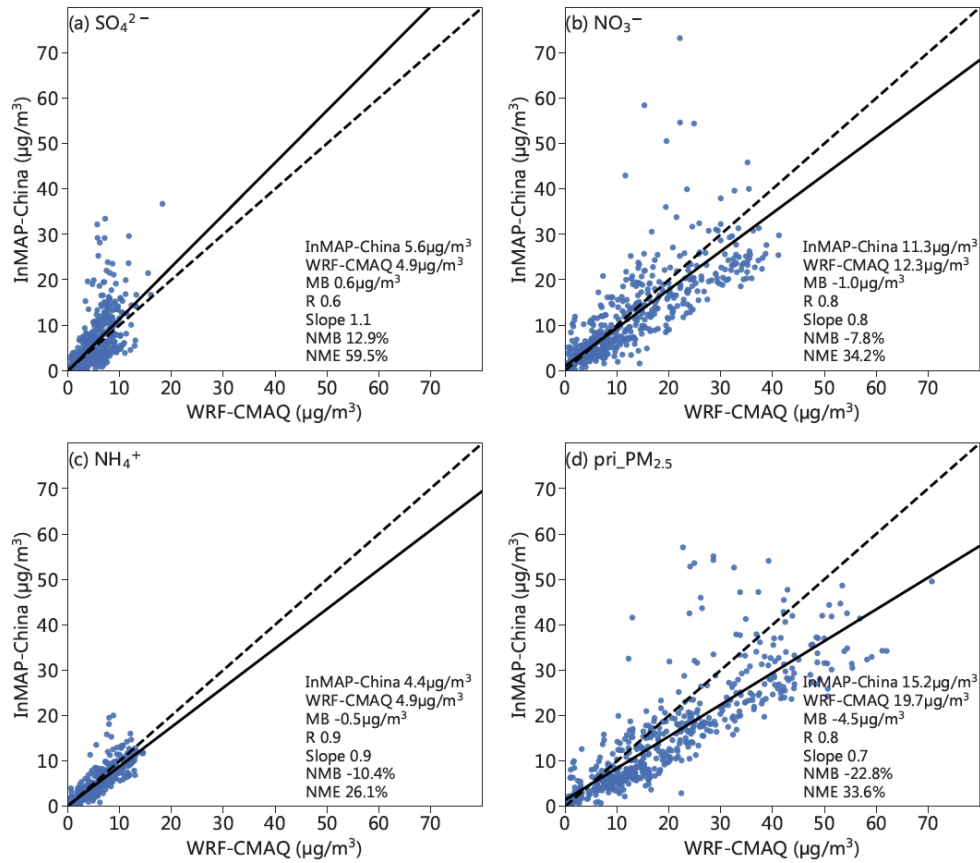
observed PM_{2.5}. The observed total PM_{2.5} concentrations are marked as circles in panel (a) and panel (c). In panel

706

(d), the circle shows the difference between the PM_{2.5} simulated by InMAP-China and the observed PM_{2.5}. The same

707

color bar is utilized in the contour and the marked circle.

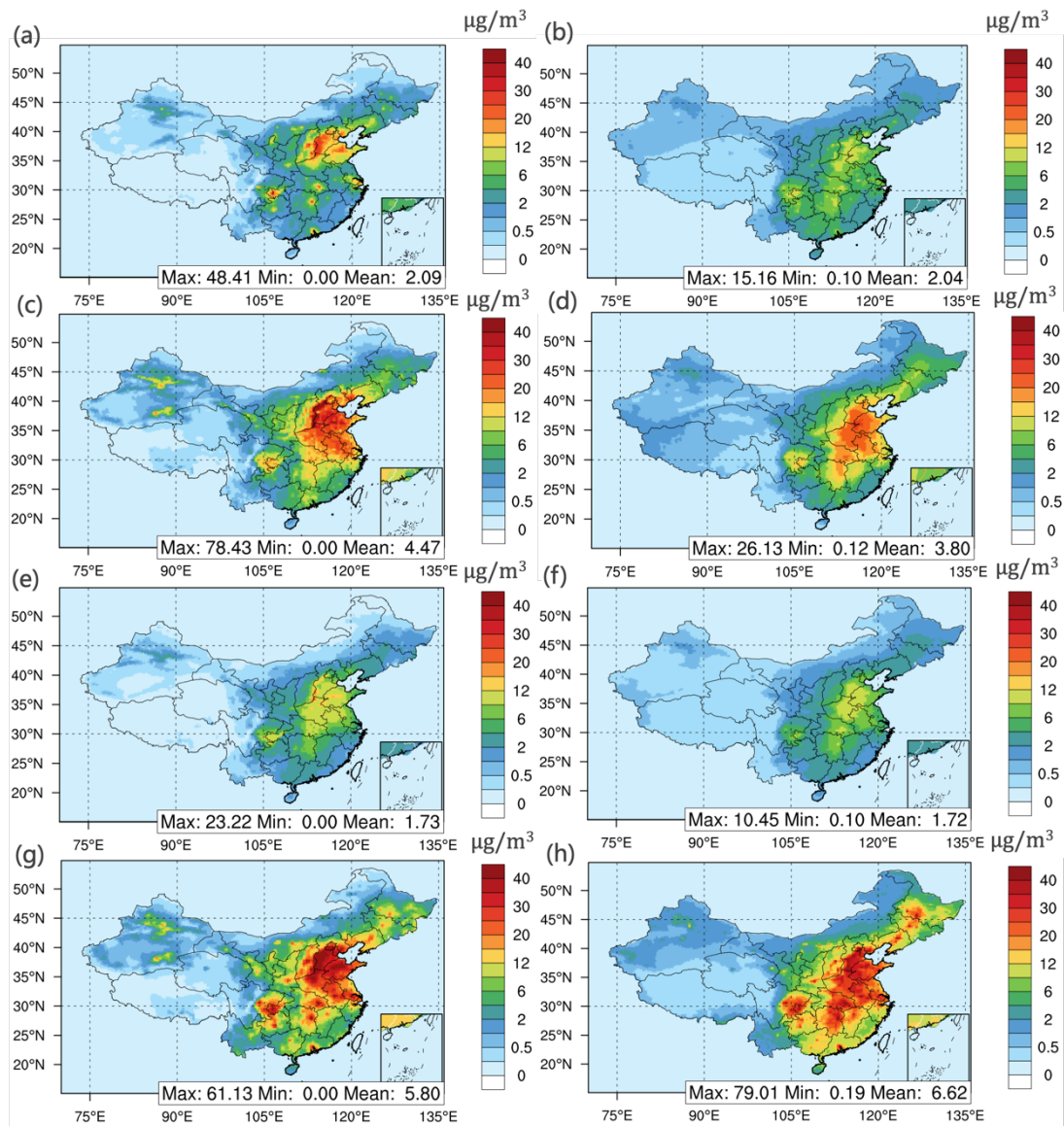


708

709 **Figure 4 Scatter plot comparing the PM_{2.5} composition concentration modelled by the InMAP-China and**

710 **WRF-CMAQ models.** Panels (a), (b), (c), and (d) display sulfate, nitrate, ammonium, and primary PM_{2.5},

711 respectively. The statistical metrics are labelled in the lower right corner of each panel.



712

713

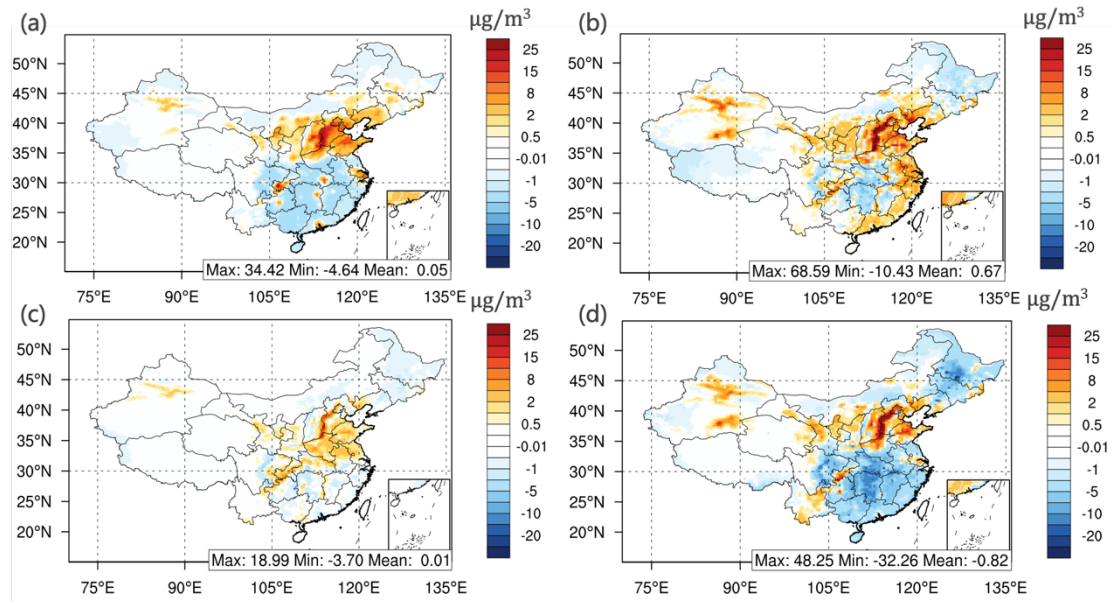
Figure 5 The spatial pattern of PM_{2.5} compositions modelled by the InMAP-China and WRF-CMAQ models.

714

Panels (a), (c), (e), and (g) present the sulfate, nitrate, ammonium, and primary PM_{2.5}, respectively, simulated by

715

InMAP-China in the InMAP-TOT scenario. Panels (b), (d), (f), and (h) present the results modelled by WRF-CMAQ.



716

717

Figure 6 The difference in the spatial pattern of PM_{2.5} compositions between InMAP-China and WRF-CMAQ.

718

Panels (a), (b), (c), and (d) display sulfate, nitrate, ammonium, and primary PM_{2.5}, respectively.

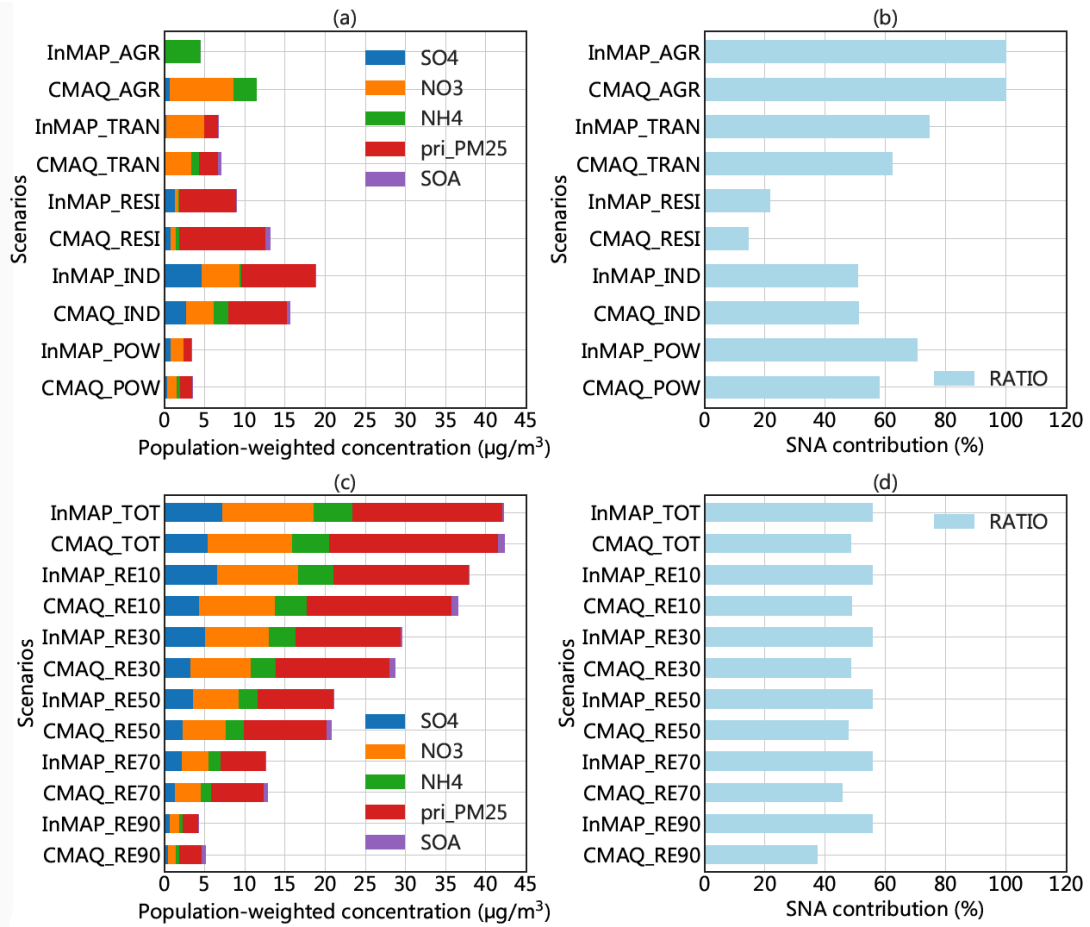
719

720

721

722

723



724

725

Figure 7 Comparison of PM_{2.5} component concentrations and SNA contributions in these eleven simulations.

726

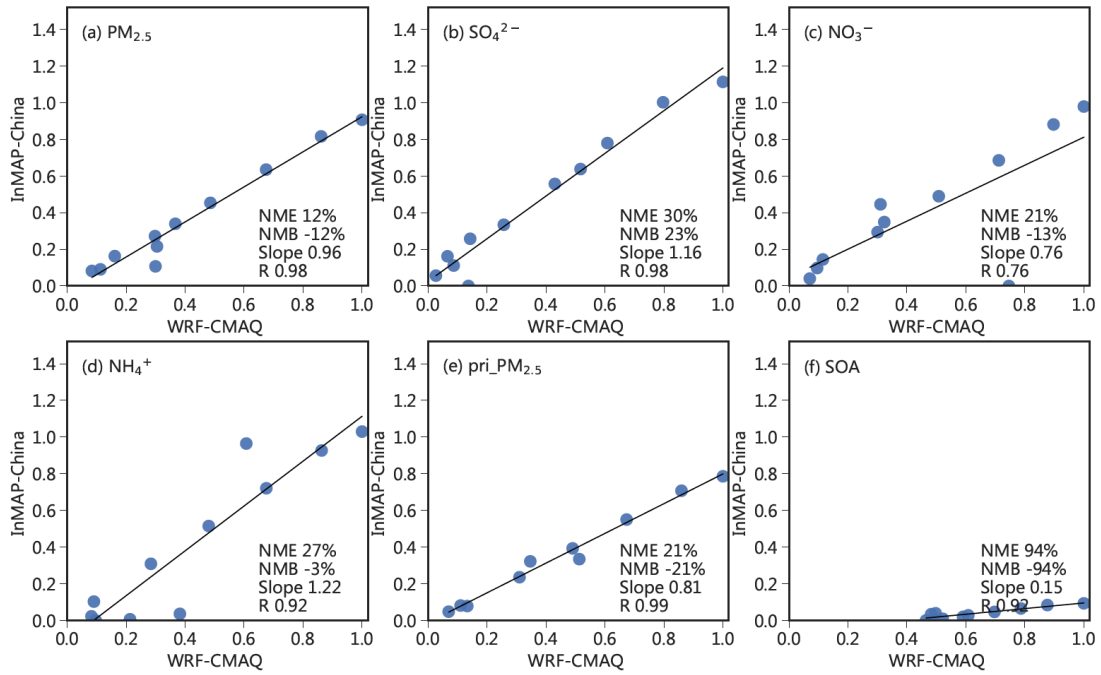
(a) and (c) show the modelled PM_{2.5} compositions. Panel (a) presents the results of sectoral emission scenarios, and

727

panel (c) presents the results of the baseline and emission abatement scenarios. Panels (b) and (d) present the SNA

728

contribution (%) for each scenario.



729

730

Figure 8 Marginal change in nationwide annual average population-weighted $PM_{2.5}$ concentration and its

731

composition as modelled by InMAP-China and WRF-CMAQ for eleven emissions scenarios. The population-

732

weighted pollutant concentration for each scenario is normalized using the largest value among all scenarios

733

modelled by CMAQ. The eleven dots represent the eleven scenarios, and the statistical metrics are labelled in the

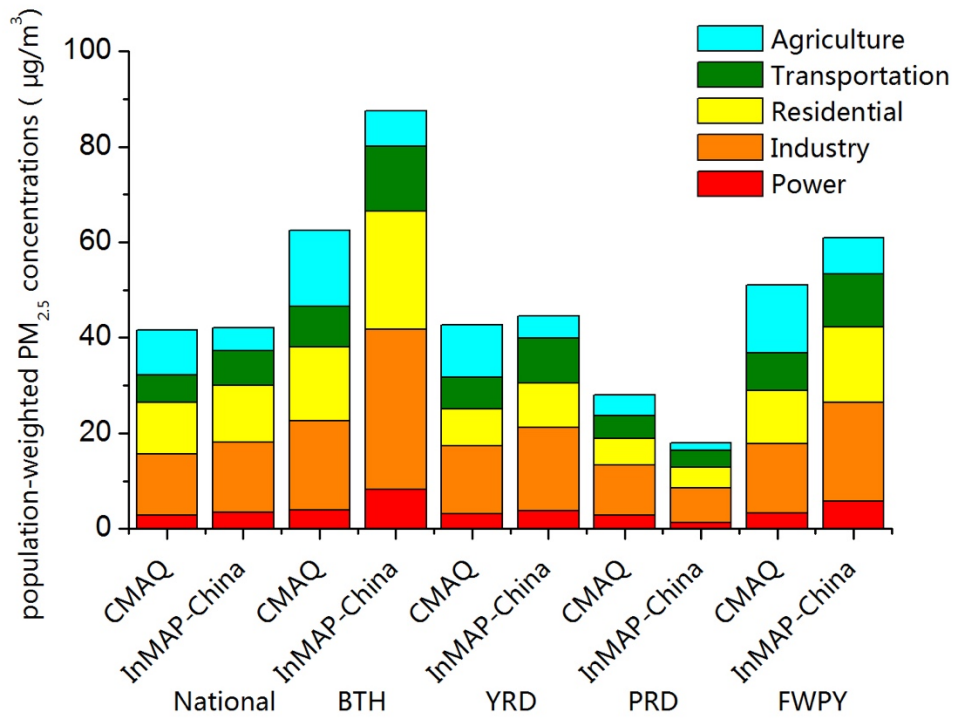
734

lower right corner for each panel.

735

736

737



738

739 **Figure 9 Comparison of source contributions to population-weighted PM_{2.5} concentrations estimated by the**
 740 **two models.**

741

742

743

744

745

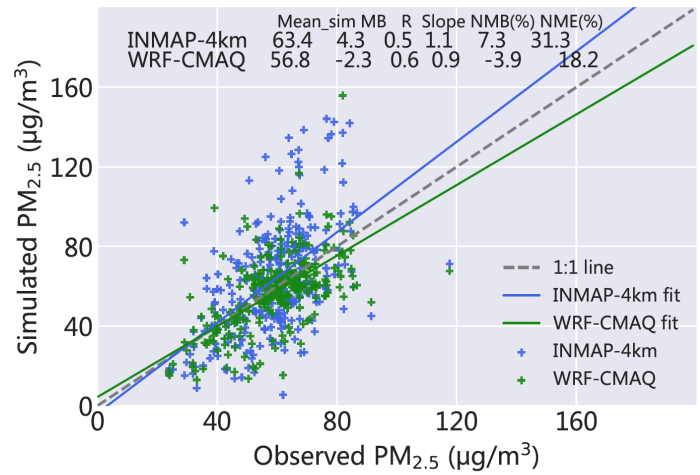
746

747

748

749

750



751

752 **Figure 10 Scatter plot comparing the PM_{2.5} concentration modeled in the BTH region with 4 km spatial**

753 **resolution by the InMAP-China and WRF-CMAQ. The value of statistical metrics is labeled in the panel.**

754

755

756

757

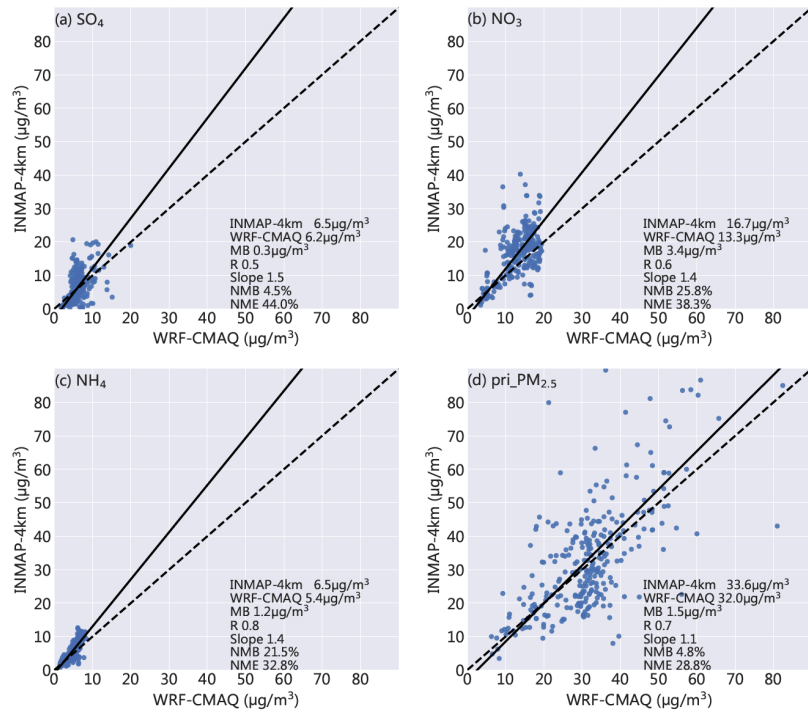
758

759

760

761

762



763

764 **Figure 11 Scatter plot comparing the $\text{PM}_{2.5}$ composition concentration modeled at BTH region with 4km**

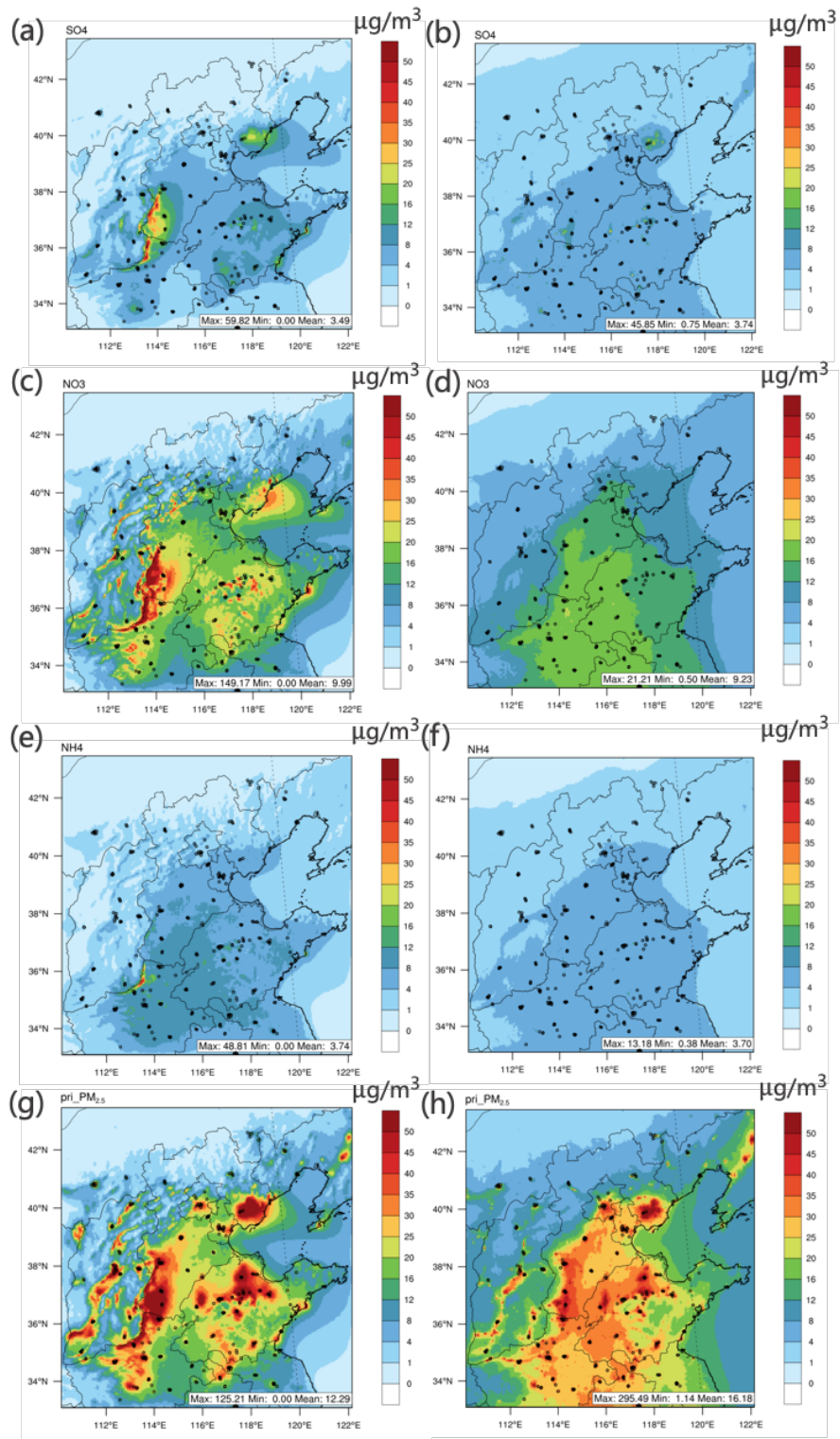
765 **spatial resolution by the InMAP-China and WRF-CMAQ. Panels (a), (b), (c) and (d) display the sulfate, nitrate,**

766 **ammonium, and primary $\text{PM}_{2.5}$, respectively. The statistical metrics are labeled in the lower right corner of each**

767 **panel.**

768

769



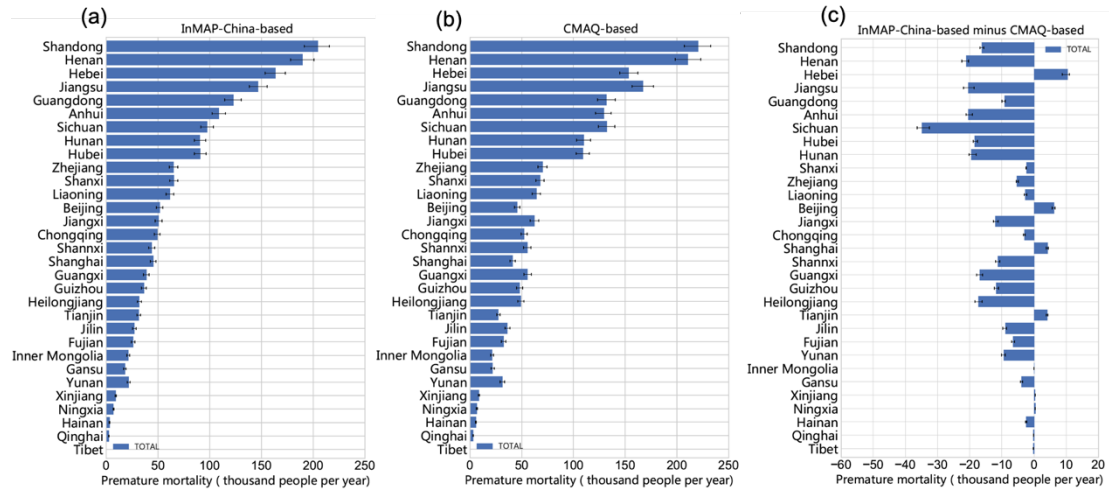
770

771 **Figure 12 The spatial pattern of PM_{2.5} compositions simulated in the BTH region with 4km spatial resolution**

772 **by the InMAP-China and WRF-CMAQ. Panels (a), (c), (e), and (g) present the sulfate, nitrate, ammonium, and**

773 **primary PM_{2.5}, respectively, simulated by InMAP-China. Panels (b), (d), (f), and (h) present the corresponding**

774 **results simulated by WRF-CMAQ.**



775

776 **Figure 13 Comparison of PM_{2.5}-related premature mortality using the PM_{2.5} predictions from two models.**

777 (a) InMAP-China-based; (b) CMAQ-based; and (c) difference between the two models.

778

779

780

781

782

783

784

785

786